

# Electrothermal Analyses of Bandpass NGD RLC-Network Topologies

Eric Jean Roy Sambatra<sup>1</sup>, Samuel Ngoho<sup>2</sup>, Fayrouz Haddad<sup>3</sup>, Mathieu Guerin<sup>3</sup>,  
Glauco Fontgalland<sup>4</sup>, Wenceslas Rahajandraibe<sup>3</sup>, and Blaise Ravelo<sup>5</sup>

<sup>1</sup>Institut Supérieur de Technologie (ISTD), BP 509, Antsiranana 201, Madagascar

<sup>2</sup>Association Française de Science des Systèmes (AFSCET), 151 Bd de l'Hôpital, Paris 75013, France

<sup>3</sup>Aix-Marseille University, CNRS, University of Toulon, IM2NP UMR7334, Marseille, France

<sup>4</sup>Federal University of Campina Grande, Applied Electromagnetic and Microwave Lab., Campina Grande/PB, 58429, Brazil

<sup>5</sup>Nanjing University of Information Science & Technology, School of Electronic & Information Engineering Nanjing, China 210044

Corresponding author: Fayrouz Haddad (e-mail: fayrouz.haddad@im2np.fr).

**ABSTRACT** This paper develops an original study of temperature effect on the unfamiliar bandpass (BP) negative group delay (NGD) lumped passive circuits. The paper presents the first study of electrothermal analysis of electronic circuits classified as BP-NGD topologies. The considered BP-NGD passive cells are mainly constituted by RLC-resonant networks. The equivalence between two basic BP-NGD topologies constituted by RLC-series and RLC-parallel networks is elaborated via the voltage transfer function (VTF) analogy. Then, the theoretical demonstrations are introduced to define the main specifications as the NGD center frequency, NGD value, attenuation and NGD bandwidth. The electrothermal innovative study is developed based on the temperature coefficient resistor (TCR) of elements constituting the BP-NGD circuits. With proofs of concept of RLC-series and RLC-parallel circuits operating with -500 ns NGD value at 13.56 MHz, calculated and simulated results showing are in excellent agreement. The sensitivity analyses of BP-NGD specifications in function of ambient temperature variation from 0°C to 100°C are investigated. The BP-NGD response variations versus frequency and temperature are characterized with thermo-frequency cartographies and discussed.

**INDEX TERMS** Bandpass (BP) negative group delay (NGD), Electrothermal analysis, NGD analysis, Circuit theory, Equivalent topology.

## I. INTRODUCTION

THE modern engineering progresses with more and more complex design of electronic system. To innovate such electronic system, curious scientific approaches are necessary, for example, including hybridization of monophysics as electrical and thermal approaches [1-4]. Because of metallic conductivity temperature coefficient [5], it was reported from [6-9] that different electronic components, printed circuit boards (PCBs) and devices are particularly sensitive to the temperature variation. In addition to such Multiphysics approach, modern engineers have to be open mind on unfamiliar electronic function as the case of negative group delay (NGD) [10-28]. Despite the performed available in the literature, few electronic design, fabrication, test and sale engineers are nowadays familiar to this counterintuitive NGD function. For this reason, different sections on the investigation on the NGD effect are hereafter described.

The transposition of 3-D to 1-D structure enables to design transmission line (TL) based left-handed (LF)

microwave circuit operating with negative refractive index (NRI) periodical structure [10-12]. For the further clarity about the analytical mechanism of the NGD effect, we can imagine the case of dispersive media with effective group index, as the case of LH metamaterials [10-12] depending on the angular frequency. It implies that the medium group velocity is a function of the group index. Because of dispersion around resonance frequency around certain wavelengths, we may realize NGD. To interpret in more practical way the NGD, we imagine a wave signal modulating harmonic sine signal with frequency.

The interpretation of the NGD effect in the optical area intrigues different scientific communities as the radio frequency (RF) and microwave engineers. Therefore, the NGD effect was also studied with microwave circuit design by using LH metamaterial TL based circuit [10-12]. Research efforts were deployed on the design, implementation and measurement of NGD microwave circuits [13-20]. The main challenges on the NGD research works of the two last decades were focused on the

designability [10-20], the NGD asymptotic limits [14], the implementation of NGD active topologies [13-15], the circuit performances as low attenuation loss and compact [16-19] microwave circuits. The extremely wide diversity of NGD circuit design with TL based compact microstrip topologies [10-12,17-19], absorptive stop-band filter [29] and interference techniques [20] answers to the NGD existentiality question. In the same period of the microwave circuit elaboration, RLC-resonant network based NGD investigation in low frequencies (LFs) was also performed [21-22].

The most developed study on the existence, theorization, simulation and experimentation of the NGD function was performed with lumped electronic circuits [21-28]. In this case, the NGD electronic circuits were designed with R, L and C lumped active topologies [14-17]. From circuit analysis, it was shown theoretically and experimentally that the NGD effect signature in the time-domain enables to realize an extraordinary and undeniably signal superluminal propagation with output signal peaks and slopes in time-advance compared to the corresponding input [23-25]. Despite this counterintuitive phenomenon, it was emphasized that the NGD signal propagation does not violate the Einstein causality principle [21-24]. But so far, because of the counterintuitive effect related to the time delay, the meaning of the NGD function is currently not yet adopted by majority of electronic engineers. Simpler theory of NGD function was established by the analogy between the filter behavior [26-28]. Similar to the filter analysis, the concrete implementation of the previous BP-NGD ideal response must start with the calculation of voltage transfer function (VTF). Then, we will propose a BP-NGD transfer function (TF) canonical form [29]. Depending on the positioning of the NGD frequency bands, we can have NGD low-pass [26-27], high-pass [28], and bandpass (BP) [26,29] NGD functions. A lot of challenge in terms of theory, design, fabrication and test remain to be overcome for NGD circuits. We are answering to the extra-question on the NGD specification temperature effect as conducted for the GaN field effect transistors [1-3], integrated circuit performance [4] and microstrip distributed interconnects [6-9]. Therefore, we are exploring in the first time, the electrothermal NGD analysis of lumped passive circuit in the present research work.

The present paper contributes originally on the BP-NGD function analysis by considering RLC-resonant network-based two passive topologies. The main novelty of the paper concerns the temperature coefficient resistor (TCR) effect on the BP-NGD specifications. The paper is outlined follows:

- Section 2 introduces the analytical characteristics of the RLC-network based BP-NGD topologies. The BP-NGD theory of the RLC resonant networks is elaborated from the equivalent voltage transfer

function (VTF) between the RLC-series and RLC-parallel resonant networks based passive topologies.

- Section 3 establishes the analytical expressions demonstrating how the TCR influences the BP-NGD specifications.
- Section 4 is focused on the proof of concept (POC) investigation which illustrates why the considered topologies behave as BP-NGD function.
- Section 5 investigates on numerical applications based on the mapping versus electrothermal parameters will be presented. The variations of the BP-NGD responses will be discussed in the considered range of ambient temperature.
- Finally, Section 6 ends the paper with a conclusion.

## II. ANALYTICAL CHARACTERISTICS OF THE CONSIDERED BP-NGD CIRCUIT

This section describes the BP-NGD theory of the two different RLC-resonant network passive topologies under study. The analytical elaboration and the BP-NGD function specifications are established in [26,29].

### A. DESCRIPTION OF BP-NGD CIRCUIT TOPOLOGIES UNDER STUDY

Fig. 1(a) and Fig. 1(b) represent the schematic diagram of the RLC-series and RLC-parallel network-based passive topologies under study.

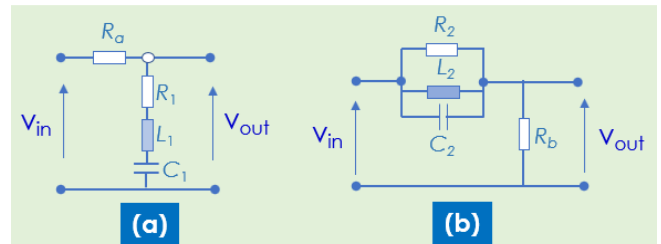


FIGURE 1. (a) RLC-series and (b) RLC-parallel network-based BP-NGD topologies.

By denoting the Laplace variable,  $s$ , the topology shown in Fig. 1(a) is constituted by a series resistance,  $R_a$ , and parallel impedance of RLC-series network:

$$Z_1(s) = R_1 + L_1s + \frac{1}{C_1s}. \quad (1)$$

The other topology shown in Fig. 1(b) is constituted by a parallel resistance,  $R_b$ , and a series impedance composed of RLC-parallel network:

$$Z_2(s) = \frac{1}{\frac{1}{R_2} + \frac{1}{L_2s} + C_2s}. \quad (2)$$

These RLC-series and RLC-parallel topologies exploited in the present paper are analyzed from the VTF defined by  $T(s) = V_{out}(s) / V_{in}(s)$ .

**B. CANONICAL FORM OF BP-NGD FUNCTION AND EQUIVALENCE BETWEEN RLC-SERIES AND RLC-PARALLEL VTFs**

As primordial step of the present study, we consider the BP-NGD TF canonical form defined by the second order polynomial formula [29]:

$$T(s) = \frac{s^2 + \omega_n s + \omega_0^2}{s^2 + \omega_d s + \omega_0^2} \quad (3)$$

with the characteristic parameters are the positive real coefficients representing the NGD center angular frequency,  $\omega_0$ , and the numerator/denominator angular frequency,  $\omega_n$ , and  $\omega_d$ . By polynomial mathematical identification, we can define the BP-NGD canonical form parameters of RLC-series and RLC-parallel topologies indicated in Table I.

**TABLE I.** PARAMETERS OF BP-NGD CANONICAL FORM OF RLC-SERIES AND RLC-PARALLEL TOPOLOGIES

Designation	RLC-series	RLC-parallel
NGD center frequency	$\omega_{0a} = \frac{1}{\sqrt{L_1 C_1}}$ (4)	$\omega_{0b} = \frac{1}{\sqrt{L_2 C_2}}$ (7)
Numerator parameter	$\omega_{na} = \frac{R_1}{L_1}$ (5)	$\omega_{nb} = \frac{1}{R_2 C_2}$ (8)
Denominator parameter	$\omega_{da} = \frac{R_1 + R_a}{L_1}$ (6)	$\omega_{db} = \frac{R_2 + R_b}{R_2 R_b C_2}$ (9)

The equivalence between the VTF of the RLC-series and RLC-parallel topologies lead to the following condition:

$$\omega_{0a} = \omega_{0a} \quad (10a)$$

$$\omega_{na} = \omega_{nb} \quad (10b)$$

$$\omega_{da} = \omega_{db} \quad (10c)$$

Given RLC-series and by fixing resistance,  $R_b$ , we have the following relationship from the previous equation system:

$$R_2 = \frac{R_a R_b}{R_1} \quad (11)$$

$$L_2 = R_a R_b C_1 \quad (12)$$

$$C_2 = \frac{L_1}{R_a R_b} \quad (13)$$

**C. NGD CHARACTERIZATION FROM BP-NGD CANONICAL FORM**

The specific expressions of the BP-NGD parameters appropriated to the VTF canonical form defined in [29] is used in the present study. The frequency responses represented by the magnitude and GD were calculated. At the NGD center frequency, we have the GD value [29]:

$$GD_n = \frac{2(\omega_n - \omega_d)}{\omega_n \omega_d} \quad (14)$$

It means that the GD is negative when:

$$\omega_n < \omega_d \Leftrightarrow \frac{\omega_n}{\omega_d} < 1. \quad (15)$$

We can remark that this condition is always satisfied with the RLC network-based topologies by considering the parameters defined in Table I. Moreover, the magnitude of the VTF is not equal to zero:

$$T_n = \frac{\omega_n}{\omega_d} \quad (16)$$

The associated cut-off frequencies obtained from equation (3) can be formulated as:

$$\omega_1 = \sqrt{\omega_c^2 + \frac{\omega_n \omega_d - \sqrt{\omega_n \omega_d (4\omega_c^2 + \omega_n \omega_d)}}{2}} \quad (17)$$

$$\omega_2 = \sqrt{\omega_c^2 + \frac{\omega_n \omega_d + \sqrt{\omega_n \omega_d (4\omega_c^2 + \omega_n \omega_d)}}{2}} \quad (18)$$

Now, we can verify in the next subsection why the topologies of circuit shown in Figs. 1 can be assumed as BP-NGD functions.

**D. BP-NGD ANALYSIS**

The proposed NGD analysis of our passive topologies consists in expressing the NGD specifications parameters in function of R, L and C.

**1) RLC-SERIES TOPOLOGY**

The NGD center and cut-off frequencies are denoted:

$$\omega_{c1} = \omega_{0a} \quad (19a)$$

$$\omega_1 = \omega_{1a} \quad (19b)$$

$$\omega_2 = \omega_{2a} \quad (19c)$$

The NGD value of the circuit introduced in Fig. 1(a) is equal to:

$$GD_{n1} = \frac{-2R_a L_1}{R_1 (R_1 + R_a)} \quad (20)$$

We can see that this GD is unconditionally negative for all parameters of the RLC-series topology. The attenuation at the NGD center frequency is equal to:

$$T_{n1} = \frac{R_1}{R_1 + R_a} \quad (21)$$

For the sake of the mathematical simplicity, the NGD BW:

$$\Delta\omega_a = \omega_{2a} - \omega_{1a} \quad (22)$$

will not be expressed in function of the R, L and C variables in the present paragraph.

**2) RLC-PARALLEL TOPOLOGY**

In this case, the NGD center frequency  $\omega_{c2} = \omega_{0b}$  are denoted:

$$\begin{cases} \omega_{c2} = \omega_{0b} \\ \omega_1 = \omega_{1b} \\ \omega_2 = \omega_{2b} \end{cases} \quad (23)$$

The NGD value of the RLC-parallel circuit is equal to:

$$GD_{n2} = \frac{-2R_2 R_b C_2}{R_2 + R_b} \quad (24)$$

Once again, we emphasize that this GD is unconditionally negative for all parameters of the RLC-parallel topology. The corresponding attenuation at the calculated NGD center frequency becomes:

$$T_{n2} = \frac{R_b}{R_2 + R_b}. \quad (25)$$

For the sake of the mathematical simplicity, the RLC-parallel topology NGD BW will not be expressed in details in function of the R, L and C variables. However, the NGD BW can be simply expressed as:

$$\Delta\omega_a = \omega_{2a} - \omega_{1a}. \quad (26)$$

Knowing these NGD parameters, we can establish an electrothermal analysis with respect to the resistance variation.

### III. ELECTROTHERMAL ANALYSIS OF RLC-RESONANT NETWORK BASED BP-NGD PASSIVE TOPOLOGIES

The present section introduces the temperature influence on the BP-NGD responses. The study will be focused essentially on the TCR linear effect on the resistive components.

#### A. TEMPERATURE LINEAR VARIATION HYPOTHESIS

The study is focused on the cases of linear variations of the temperature effect. Accordingly, our electrothermal analysis is formulated with the resistance variation in function of the ambient temperature:

$$\theta = \theta_0 + \Delta\theta. \quad (27)$$

By denoting the initial reference temperature denoted  $\theta_0 = 25^\circ\text{C}$  and the temperature variation,  $\Delta\theta > 0$ . We denote  $\lambda$  the TCR of all the resistances constituting our NGD circuits. Then, the temperature effect on the inductance and capacitance is supposed negligible.

Based on this hypothesis, we have the BP-NGD electrothermal analytical investigation in the next paragraphs.

#### B. ANALYTICAL EXPRESSION OF TCR EFFECT ON THE RLC-SERIES NGD RESPONSES

As the first case of study, we considered the BP-NGD topology constituted by RLC-series network. The analytical electrothermal BP-NGD investigation are developed in the following paragraphs. The effect of TCR is analytically described in this subsection.

##### 1) RESISTANCE VARIATION LAW

With the above defined TCR, the resistances of RLC-series circuit are varying linearly with the traditional relation defined as:

$$R_a(\theta) = R_a(1 + \lambda \cdot \Delta\theta) \quad (28)$$

$$R_1(\theta) = R_1(1 + \lambda \cdot \Delta\theta). \quad (29)$$

From these relations, the corresponding absolute variations of the resistances are written as, respectively:

$$\Delta R_a(\theta) = \lambda \cdot \Delta\theta R_a(\theta_0) \quad (30)$$

$$\Delta R_1(\theta) = \lambda \cdot \Delta\theta \cdot R_1(\theta_0). \quad (31)$$

We will exploit these resistance variations to analyze the temperature influences on the BP-NGD parameters of our RLC-series topology.

##### 2) TCR EFFECT ON GD AND ATTENUATION

By taking into account these variations, we can rewrite the GD value expressed in equation (20) as:

$$GD_{n1}(\theta) = \frac{-2R_a(1 + \lambda\Delta\theta)L_1}{R_1(1 + \lambda\Delta\theta)[R_1(1 + \lambda\Delta\theta) + R_a(1 + \lambda\Delta\theta)]} \quad (32)$$

which can be simplified as:

$$GD_{n1}(\theta) = \frac{-2R_a L_1}{R_1(1 + \lambda\Delta\theta)(R_1 + R_a)}. \quad (33)$$

By considering equation (20), this last formula can be simplified as:

$$GD_{n1}(\theta) = \frac{GD_{n1}(\theta_0)}{1 + \lambda\Delta\theta} = \frac{GD_{n1}(\theta_0)}{1 + \lambda(\theta - \theta_0)}. \quad (34)$$

The absolute variation of the GD value is given by:

$$\Delta GD_{n1}(\theta) = \frac{\lambda \cdot \Delta\theta \cdot GD_{n1}(\theta_0)}{1 + \lambda\Delta\theta}. \quad (35)$$

The electrothermal investigation applied to the magnitude implies the modification of equation (21) as follows:

$$T_{n1}(\theta) = \frac{R_1(1 + \lambda\Delta\theta)}{R_1(1 + \lambda\Delta\theta) + R_a(1 + \lambda\Delta\theta)} = T_{n1}(\theta_0). \quad (36)$$

We can point out that the RLC-series topology attenuation variation,  $\Delta T_{n1}(\theta) = 0$ , should not depend on the temperature one.

##### 3) TCR EFFECT ON BP-NGD BW

The NGD BW variation can be estimated from the variations of numerator and denominator of the BP-NGD canonical form in function of the resistance variations:

$$\Delta\omega_{na}(\theta) = \frac{\Delta R_1(\theta)}{L_1} \quad (37)$$

$$\Delta\omega_{da}(\theta) = \frac{\Delta R_1(\theta) + \Delta R_a(\theta)}{L_1}. \quad (38)$$

In function of temperature variation, the two previous equations become:

$$\Delta\omega_{na}(\theta) = \frac{R_1(\theta_0)\lambda\Delta\theta}{L_1} \quad (39)$$

$$\Delta\omega_{da}(\theta) = \frac{[R_1(\theta_0) + R_a(\theta_0)]\lambda\Delta\theta}{L_1}. \quad (40)$$

The NGD center frequency remains constant because we assume that  $L_1$  and  $C_1$  do not change with the temperature. Therefore, the BW variation can be written as:

$$\Delta[\Delta\omega_a(\theta)] = \Delta\omega_{2a}(\theta) - \Delta\omega_{1a}(\theta) \quad (41)$$

with:

$$\Delta\omega_{1a}(\theta) \approx \frac{\partial\omega_{1a}}{\partial\omega_{na}} \Delta\omega_{na}(\theta) + \frac{\partial\omega_{1a}}{\partial\omega_{da}} \Delta\omega_{da}(\theta) \quad (42)$$

$$\Delta\omega_{2a}(\theta) \approx \frac{\partial\omega_{2a}}{\partial\omega_{na}} \Delta\omega_{na}(\theta) + \frac{\partial\omega_{2a}}{\partial\omega_{da}} \Delta\omega_{da}(\theta). \quad (43)$$

Substituting, equation (39) into equation (42), and equation (40) into equation (43), we have the two last expressions rewritten as, respectively:

$$\Delta\omega_{1a}(\theta) \approx \frac{\lambda\Delta\theta}{L_1} \left\{ \begin{array}{l} R_1(\theta_0) \frac{\partial\omega_{1a}}{\partial\omega_{na}} + \\ [R_1(\theta_0) + R_a(\theta_0)] \frac{\partial\omega_{1a}}{\partial\omega_{da}} \end{array} \right\} \quad (44)$$

$$\Delta\omega_{2a}(\theta) \approx \frac{\lambda\Delta\theta}{L_1} \left\{ \begin{array}{l} R_1(\theta_0) \frac{\partial\omega_{2a}}{\partial\omega_{na}} + \\ [R_1(\theta_0) + R_a(\theta_0)] \frac{\partial\omega_{2a}}{\partial\omega_{da}} \end{array} \right\}. \quad (45)$$

The same approach of the BP-NGD parameter temperature effect applied to the RLC-parallel circuit will be investigated in the next paragraph.

### C. ANALYTICAL EXPRESSION OF TCR EFFECT ON THE RLC-PARALLEL NGD RESPONSES

The second case of electrothermal study is focused on the BP-NGD circuit based on the RLC-parallel network.

#### 1) TCR EFFECT ON THE CONSTITUTING ELEMENTARY RESISTORS

In this case, the two constituting resistances of the RLC-parallel NGD circuit change according to the following linear law:

$$R_b(\theta) = R_b(1 + \lambda \cdot \Delta\theta) \quad (46)$$

$$R_2(\theta) = R_2(1 + \lambda \cdot \Delta\theta). \quad (47)$$

The corresponding absolute variations are written as, respectively:

$$\Delta R_b(\theta) = \lambda \cdot \Delta\theta \cdot R_b(\theta_0) \quad (48)$$

$$\Delta R_2(\theta) = \lambda \cdot \Delta\theta \cdot R_2(\theta_0). \quad (49)$$

These relations will serve to the analysis of the RLC-parallel topology.

#### 2) TCR EFFECT ON THE GD AND ATTENUATION

Similar to the previous case of RLC-series network, we can exploit the GD expression at the NGD center frequency. Accordingly, the GD value expressed in equation (20) is transformed as:

$$GD_{n_2}(\theta) = \frac{-2R_2 R_b C_2 (1 + \lambda\Delta\theta)}{R_2 + R_b} \quad (50)$$

which can be simplified as:

$$GD_{n_2}(\theta) = (1 + \lambda\Delta\theta)GD_{n_2}(\theta_0) \quad (51)$$

or

$$GD_{n_2}(\theta) = [1 + \lambda(\theta - \theta_0)]GD_{n_2}(\theta_0) \quad (52)$$

The absolute variation of the GD value is given by:

$$\Delta GD_{n_2}(\theta) = \lambda \cdot \Delta\theta \cdot GD_{n_2}(\theta_0). \quad (53)$$

We can underline from this last expression that the GD value variation of the second topology is proportional to the temperature variation. This effect is the inverse of the previous case RLC-series topology. The magnitude changes following substituting the resistances of equation (30) and equation (31) substituted in equation (21):

$$T_{n_2}(\theta) = \frac{R_b(1 + \lambda\Delta\theta)}{R_2(1 + \lambda\Delta\theta) + R_b(1 + \lambda\Delta\theta)} = T_{n_2}(\theta_0). \quad (54)$$

The attenuation variation,  $\Delta T_{n_2}(\theta) = 0$ , should not depend on the temperature one.

#### 3) TCR EFFECT ON BP-NGD BW

The NGD BW sensitivity for the RLC parallel topology can be estimated from the variations of numerator and denominator of the BP-NGD canonical form in function of the resistance variations:

$$\Delta\omega_{nb}(\theta) = \frac{\Delta R_2(\theta)}{L_2} \quad (55)$$

$$\Delta\omega_{db}(\theta) = \frac{\Delta R_2(\theta) + \Delta R_b(\theta)}{L_2}. \quad (56)$$

These two equations can be rewritten as follows to express the numerator and denominator parameter absolute variation:

$$\Delta\omega_{nb}(\theta) = \frac{R_2(\theta_0)\lambda\Delta\theta}{L_2} \quad (57)$$

$$\Delta\omega_{db}(\theta) = \frac{\lambda \cdot \Delta\theta [R_2(\theta_0) + R_b(\theta_0)]}{L_2}. \quad (58)$$

The NGD center frequency because we assume that  $L_1$  and  $C_1$  do not change with the temperature. Therefore, the BW variation can be written as:

$$\Delta[\Delta\omega_b(\theta)] = \Delta\omega_{2b}(\theta) - \Delta\omega_{1b}(\theta) \quad (59)$$

with

$$\Delta\omega_{1b}(\theta) \approx \frac{\partial\omega_{1b}}{\partial\omega_{nb}} \Delta\omega_{nb}(\theta) + \frac{\partial\omega_{1b}}{\partial\omega_{db}} \Delta\omega_{db}(\theta) \quad (60)$$

$$\Delta\omega_{2b}(\theta) \approx \frac{\partial\omega_{2b}}{\partial\omega_{nb}} \Delta\omega_{nb}(\theta) + \frac{\partial\omega_{2b}}{\partial\omega_{db}} \Delta\omega_{db}(\theta). \quad (61)$$

Substituting, equation (57) into equation (60), and equation (58) into equation (61), we have the two last expressions rewritten as, respectively:

$$\Delta\omega_{1b}(\theta) \approx \frac{\lambda \cdot \Delta\theta}{L_2} \left\{ \begin{array}{l} R_2(\theta_0) \frac{\partial\omega_{1b}}{\partial\omega_{nb}} + \\ [R_2(\theta_0) + R_b(\theta_0)] \frac{\partial\omega_{1b}}{\partial\omega_{db}} \end{array} \right\} \quad (62)$$

$$\Delta\omega_{2b}(\theta) \approx \frac{\lambda \cdot \Delta\theta}{L_2} \left\{ \begin{array}{l} R_2(\theta_0) \frac{\partial\omega_{2b}}{\partial\omega_{nb}} + \\ [R_2(\theta_0) + R_b(\theta_0)] \frac{\partial\omega_{2b}}{\partial\omega_{db}} \end{array} \right\}. \quad (63)$$

#### D. THEORETICAL INFERRING REMARK ON THE BP-NGD PARAMETER VARIATIONS WITH RESPECT TO THE TEMPERATURE

For both topologies, we can emphasize from the present electrothermal study that:

- Because of the resistance variation, the GD value changes with respect to the temperature. But the change behaves differently for the two RLC-resonant network topologies.
- The NGD circuit attenuation remains insensitive to the temperature variation at the center frequency.

To verify the feasibility of the developed electrothermal BP-NGD theory, PoC practical investigation will be presented in the next section.

#### IV. SIMULATED VALIDATIONS OF THE ELECTROTHERMAL BP-NGD ANALYSIS APPLIED TO RLC-RESONANT BASED CIRCUIT

The present section deals with the validation of the electrothermal BP-NGD topology. After the PoC description, the calculated and simulated results will be discussed.

##### A. POC DESIGN DESCRIPTION

The present NGD engineering was designed in two successive steps for the RLC-series circuit. Then, the RLC-parallel circuit parameters were extracted from the RLC-series ones.

##### 1) CHOICE AND CALCULATION OF RLC-NETWORK CIRCUIT PARAMETERS

The present PoC of NGD circuits are expected to operate around the RFID standard frequency,  $f_c=13.56$  MHz, NGD value,  $GD_n=-0.5$   $\mu$ s and optimal attenuation,  $T_n=-3$  dB. We first design the RLC-series circuit by using discrete components,  $R_a$ ,  $R_1$ ,  $L_1$  and  $C_1$ , with nominal values available in E24 component series. Then, the RLC-parallel series components,  $R_2$ ,  $L_2$  and  $C_2$ , were calculated by using formulas (11), (12) and (13). Then, the circuits were designed in the electronic circuit simulator ADS® environment from Keysight Technologies® as described in the following paragraph.

##### 2) ADS® DESIGN OF THE BP-NGD CIRCUIT POCs

Fig. 2(a) and Fig. 2(b) represent the schemes of the designed RLC-series and RLC-parallel circuits, respectively. Port<sub>1</sub> (resp. Port<sub>3</sub>) represents the inputs of RLC-series (resp. RLC-parallel) circuits. The outputs are respectively Port<sub>2</sub> (resp. Port<sub>4</sub>). The values of the components indicated in Table II were assigned in function of the choice made in the previous paragraph. The AC or frequency domain analysis was considered in order to simulate the magnitude, phase and GD. The minimal and maximal temperature variation parameters are also addressed in Table II. The TCR was chosen for the typical iron resistance.

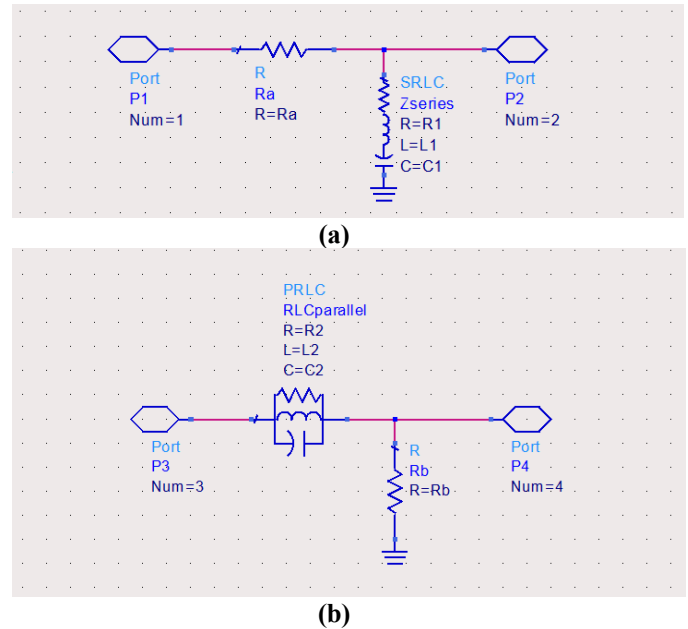


FIGURE 2. ADS® schematic of designed (a) RLC-series and (b) RLC-parallel circuits.

TABLE II. Components Used to Design the RLC-Series and RLC-Parallel Circuits

Function	Type	Parameters	Values
RLC-series circuit	Resistance	$R_a$	10 $\Omega$
		$R_1$	24 $\Omega$
	Inductance	$L_1$	20 $\mu$ H
	Capacitance	$C_1$	6.9 pF
RLC-parallel circuit	Resistance	$R_b$	290 $\Omega$
		$R_2$	120.8 $\Omega$
	Inductance	$L_2$	20 nH
	Capacitance	$C_2$	6.9 nF
Frequency	Minimal value	$f_{min}$	13 MHz
	Maximal value	$f_{max}$	14 MHz
	Sampling	-	300
Temperature	Minimal value	$\Delta\theta_{min}$	0°C
	Maximal value	$\Delta\theta_{max}$	100°C
	Sampling	-	25
	TCR(Fe)	$\lambda = \lambda_{Fe}$	$65.14 \times 10^{-4}$

The corresponding layouts designed in the Momentum environment of ADS® by using surface mounted device (SMD) lumped and normalized components which present 1206 physical size are proposed in Figs. 3. This hybrid technology PCB layout is Copper (Cu) metallized and printed on FR4 substrate with 4.4 relative permittivity and 1.6 mm thickness. It can be seen in Fig. 3(a) and Fig. 3(b) that capacitor  $C_1$  and resistor  $R_b$  are terminated by via ground (GND), respectively.

From these PoCs, validation study was performed. The following section will discuss on the obtained results.

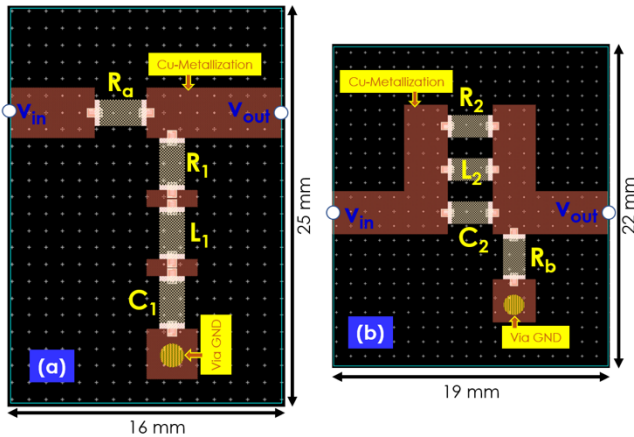


FIGURE 3. Momentum® layouts of designed (a) RLC-series and (b) RLC-parallel PoC circuits.

### B. CONTEXT OF COMPUTATION AND SIMULATION

The main question to be answered at this stage of validation study for non-specialist electronic engineers is how to verify if the proposed circuit operates as a BP-NGD function. To answer to this curious question, the numerical validation of the circuit PoCs introduced previously is explored in the present subsection. The PoC RLC-series and RLC-parallel circuit responses were calculated with MATLAB® by considering the VTF canonical form proposed in equation (3) and the parameters recapitulated in Table II. The calculation was made by means of the center frequency, numerator and denominator parameters shown in Table III. The calculations and PCB POC simulations were carried out in the frequency band from minimal bound  $f_{min}=13$  MHz to maximal bound  $f_{max}=14$  MHz with 300 and 40 sampling.

TABLE III. Canonical Form VTF Parameters

Approach	$f_c$	$f_n$	$f_d$
RLC-series	13.56 MHz	191 kHz	271 kHz
RLC-parallel	13.55 MHz	553 kHz	784 kHz

The AC simulation were run in ADS® schematic environment in the same frequency band with 40 sampling. After all computations, we obtain the results explored in the following paragraph.

### C. DISCUSSION ON THE CALCULATED AND SIMULATED BP-NGD RESPONSES

Figs. 4 depict the comparisons of the calculated and simulated results. These theoretically calculated responses represent the VTF GDs (Fig. 4(a)), magnitudes (Fig. 4(b)) and phases (Fig. 4(c)) of RLC-series and RLC-parallel results of circuit PoCs. The calculated results are represented by “Calc<sub>RLCs</sub> solid red curve” and “Calc<sub>RLCp</sub> dashed blue curve”, and the ADS® simulated results are represented by “ADS<sub>RLCs</sub> diamond dotted sky-blue curve” and “ADS<sub>RLCp</sub> circle dotted pink curve”, respectively.

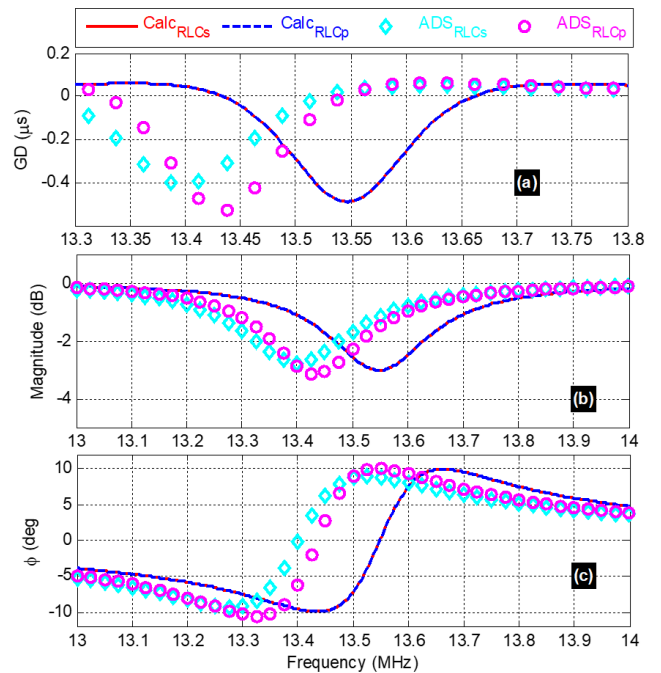


FIGURE 4. Comparisons of calculated and simulated VTFs: (a) GD, (b) magnitude and (c) phase from the RLC-series and RLC-parallel circuits shown in Figs. 2 and Figs. 3.

The simulated GD, magnitude and phase responses are only generated from the PCB circuit PoCs shown in Figs. 3. It can be pointed out that the theory and simulation results are in excellent agreement. These results confirm the equivalence between the RLC-series and RLC-parallel topologies synthesized via transformation equations (11), (12) and (13). More importantly, we can interpret from Fig. 4(a) that the considered circuits behave as a BP-NGD function. The GD is literally negative in certain frequency bands. The NGD value and NGD WB can be read from this curve. It can be seen from Fig. 4(b) that the VTF magnitude represents a typical response under similar behavior with the GD. Table IV presents the comparison of BP-NGD specifications. The phase plots displayed in Fig. 4(c) illustrate that around the NGD center frequency the phase shift is equal to zero.

TABLE IV. Comparison of BP-NGD Prototype Specifications

Approach	$f_c$	$GD_n=GD(f_c)$	$BW$	$T_n=T(f_c)$
Calc. RLC-series	13.56 MHz	-0.503 $\mu$ s	0.23 MHz	-3.05 dB
Calc. RLC-parallel	13.56 MHz	-0.503 $\mu$ s	0.23 MHz	-3.05 dB
Simu. RLC-series	13.4 MHz	-0.41 $\mu$ s	0.25 MHz	-2.79 dB
Simu. RLC-parallel	13.44 MHz	-0.53 $\mu$ s	0.225 MHz	-3.3 dB

This successful validation leads us naturally to the original electrothermal validation showing the BP-NGD robustness in the next subsection.

## V. NUMERICAL INVESTIGATION VERSUS THERMO-FREQUENCY VARIABLES

The present part of the study aims to explain the temperature stress robustness of the BP-NGD circuits discussed previously. Doing this, we assume that the circuit operates in the environment with temperature variation,  $\Delta\theta$ , from  $\Delta\theta_{\min}=0^{\circ}\text{C}$  to  $\Delta\theta_{\max}=100^{\circ}\text{C}$ . Then, only the TCR of the resistances is considered to materialize the interaction between the temperature and the circuit. We computed the magnitude and GD responses of the RLC-series and RLC-parallel circuits with respect to the couple of frequency and temperature variables by mapping the thermo-frequency cartographies. During the computation, the resistive elements of RLC-series (resp. RLC-parallel) following the linear laws given in equations (28) and (29) (resp. equations (46) and (47)).

### A. THERMO-FREQUENCY MAPPING ANALYSIS OF BP-NGD CIRCUIT MAGNITUDE RESPONSES

As results, we obtain the thermo-frequency variable cartographies of Fig. 5(a) for the VTF magnitude response of the RLC-series circuit. Then, the cartographies of Fig. 5(b) for the RLC-parallel circuit one. We observe interestingly from Fig. 5(a) that the magnitude flatness of the RLC-series circuit in the NGD bandwidth is increasing with the temperature. An inverse effect appears in Fig. 5(b) with the RLC-parallel circuit presents flatness degradation when the temperature is increasing. Fig. 5(c) shows the difference between these magnitudes of the RLC-series and RLC-parallel responses. We can see that the difference increases more considerably with the temperature. At the maximum,  $\Delta\theta=\Delta\theta_{\max}$ , we assess about 1.25 dB absolute difference.

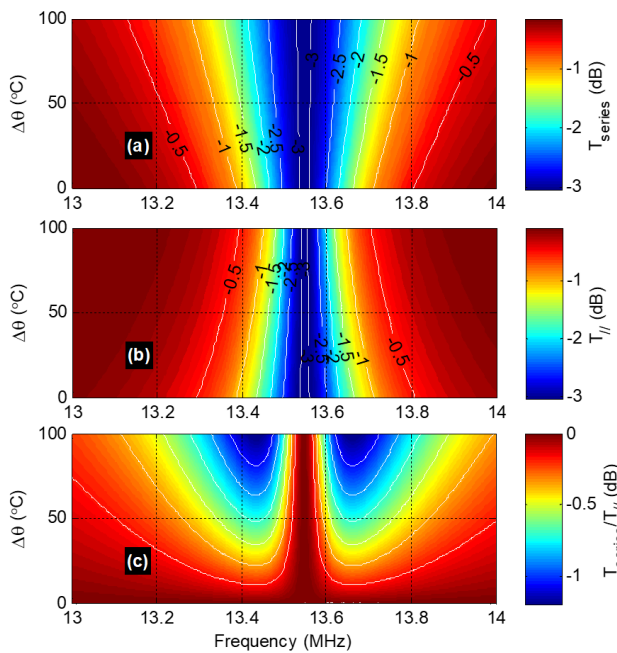


**FIGURE 5.** Thermo-frequency variable mappings of (a) RLC-series, (b) RLC-parallel VTF magnitudes and (c) ratio of both magnitudes from the circuits shown in Figs. 2.

### B. THERMO-FREQUENCY MAPPING ANALYSIS OF BP-NGD CIRCUIT GD RESPONSES

More importantly, we obtain the thermo-frequency variable cartographies of Fig. 5(a) for the GD response of the RLC-series circuit.

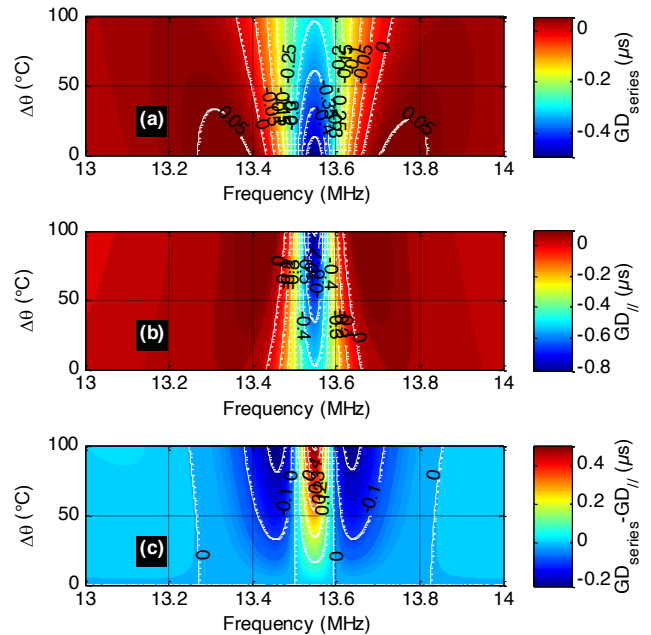


**FIGURE 6.** Thermo-frequency variable mappings of (a) RLC-series, (b) RLC-parallel VTF GDs and (c) their algebraic difference from the circuits shown in Figs. 2.

Then, the cartographies of Fig. 6(b) for the GD response of the RLC-parallel circuit. We observe interestingly:

- From Fig. 6(a) that the NGD value of the RLC-series circuit is decreasing when the temperature is increasing.
- An inverse effect appears in Fig. 6(b) with the RLC-parallel circuit presents an increase of NGD value when the temperature is increasing.

As can be seen in Fig. 6(c), the GD differences increase significantly when the temperature variation becomes higher. So even, we validate the equivalence between RLC-series and RLC-parallel in Figs. 1, both circuits react differently under ambient temperature stress.

Reaching the present step, deeper investigation on the BP-NGD specification variation with temperature is necessary. Further representation as 1D-plot at the specific NGD center frequency is discussed in the next paragraph.

### C. 1-D PLOT ELECTROTHERMAL ANALYSIS OF BP-NGD CIRCUIT MAGNITUDE AND GD RESPONSES

Fig. 7(a) confirms more clearly the statement on the GD value variation with respect to the ambient temperature stress. We can see that as expected theoretically with equation (35) and equation (51), the GD values are

changing following hyperbolic and linear variation with the temperature. The trends of variation are different with positive and negative slopes. The NGD BW variations are almost similar according to Fig. 7(b).

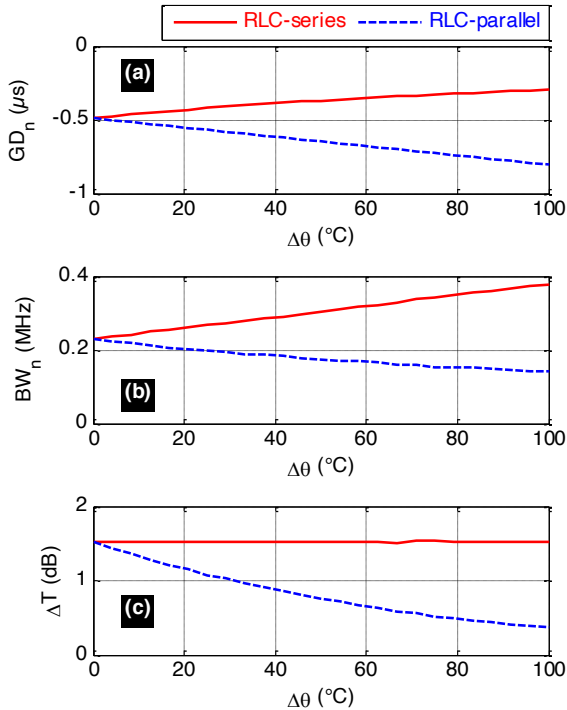


FIGURE 7. Variation of (a) NGD value and (b) NGD BW of circuits shown in Figs. 5 versus temperature variation.

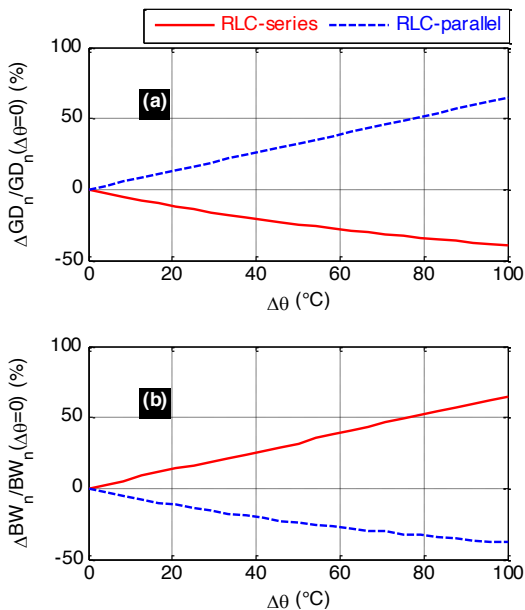


FIGURE 8. Relative variations of (a) NGD value and (b) NGD BW versus temperature variation.

The comparison of VTF magnitude flatness's,  $\Delta T$ , versus temperature variation is proposed in Fig. 7(c). We can

notice that the magnitude flatness of the RLC-series is almost negligible compared to the RLC-parallel one. The flatness of RLC-parallel VTF magnitude increases up to about 1 dB at the maximal temperature variation. The relative variations of NGD value and NGD BW are plotted in Fig. 8(a) and Fig. 8(b), respectively. Table V summarizes the NGD specifications at minimal and maximal value of the temperature.

TABLE V. BP-NGD Specifications at the Minimal and Maximal Values of Temperature Stress Variation

Circuit	$GD_n(\Delta\theta_{min})$	$BW(\Delta\theta_{min})$	$T_n(\Delta\theta_{min})$	$\Delta T(\Delta\theta_{min})$
RLC-Series	-0.489 ns	-0.23 MHz	-3.025 dB	1.519 dB
RLC-parallel	-0.489 ns	-0.23 MHz	-3.025 dB	1.519 dB
Circuit	$GD_n(\Delta\theta_{max})$	$BW(\Delta\theta_{max})$	$T_n(\Delta\theta_{max})$	$\Delta T(\Delta\theta_{max})$
RLC-Series	-0.297 ns	0.378 MHz	-3.025 dB	1.52 dB
RLC-parallel	-0.805 ns	0.142 MHz	-3.024 dB	0.38 dB

It is worth to remind that the GD is susceptible to affect the signal transmission. If the GD is positive, the output envelope appears after the input one. However, as property of BP-NGD effect, if the GD is negative the signal envelope seems in advance compared to its corresponding input [26].

## VI. CONCLUSION

An original investigation on the ambient temperature influence on BP-NGD circuits is developed. Two NGD passive topologies essentially composed of RLC-series and RLC-parallel resonant passive networks are considered.

Based on the VTF analogy, the equivalence between BP-NGD topologies constituted by RLC-series and RLC-parallel networks is established. The analytical expressions of BP-NGD specifications in function of R, L and C parameters are established. The influence of the temperature is illustrated by considering the TCR on the resistive elements of the NGD circuits. Wide variational calculus of the BP-NGD parameters for the two passive topologies are developed.

To validate, the electrothermal BP-NGD analysis of the two RLC-network circuits, comparison between theory and simulation is presented. A very good agreement between the theory and simulation which confirms the equivalent between the two considered topologies is obtained. Moreover, an innovative mapping investigation in function of the thermo-frequency variables is also introduced.

The developed electrothermal NGD study is particularly useful in the future for the BP-NGD application as for the signal integrity improvement of electronic system [30-31] in the environment with temperature effect.

## REFERENCES

- [1] V. O. Turin and A. A. Balandin, "Electrothermal simulation of the self-heating effects in GaN-based field-effect transistors," J. Appl. Phys., vol. 100, no. 5, pp. 054501-1–054501-8, Sep. 2006.

- [2] E. R. Heller and A. Crespo, "Electro-thermal modeling of multifinger AlGaIn/GaN HEMT device operation including thermal substrate effects," *Microelectron. Reliab.*, vol. 48, no. 1, pp. 45-50, Apr. 2007.
- [3] B. Shi, A. Srivastava, A. Bar-Cohen, R. Feghhi and M. Joodaki, "Thermal analysis of microwave GaN-HEMTs in conventional and flip-chip assemblies," *Int. J. RF Microw. Comput.-Aided Eng.*, vol. 28, pp. 1-14, 2018.
- [4] A. Jain, R. E. Jones, R. Chatterjee and S. Pozder, "Analytical and numerical modeling of the thermal performance of three-dimensional integrated circuits," *IEEE Trans. Adv. Packag.*, vol. 33, no. 1, pp. 56-63, May 2010.
- [5] R.A. Matula, "Electrical resistivity of Copper Gold Palladium and Silver," *J. Phys. Chem. Data*, vol. 8, no. 4, pp. 1147-1298, 1979.
- [6] B. Ravelo, A. Thakur, A. Saini and P. Thakur, "Microstrip dielectric substrate material characterization with temperature effect," *ACES Journal*, vol. 30, no. 12, pp. 1322-1328, Dec. 2015.
- [7] B. Ravelo, "Multiphysics Model of Microstrip Structure Under High Voltage Pulse Excitation," *IEEE Journal on Multiscale and Multiphysics Computational Techniques (JMMCT)*, Vol. 3, No. 1, Dec. 2018, pp. 88-96.
- [8] Z. Xu, B. Ravelo, O. Maurice, "Multiphysics Tensorial Network Analysis Applied to PCB Interconnect Fatigue Under Thermal Cycle Aggression," *IEEE Transactions on Electromagnetic Compatibility*, Vol. 61, No. 4, Aug. 2019, pp. 1253-1260.
- [9] M. N. Touzelbaev, J. Miler, Y. Yang, G. Refai-Ahmed and K. E. Goodson, "High-efficiency transient temperature calculations for applications in dynamic thermal management of electronic devices", *J. Electron. Packag.*, vol. 135, no. 3 (031001), pp. 1-8, 2013.
- [10] O. F. Siddiqui, M. Mojahedi and G. V. Eleftheriades, "Periodically Loaded Transmission Line With Effective Negative Refractive Index and Negative Group Velocity," *IEEE Trans. Antennas Propagat.*, Vol. 51, No. 10, Oct. 2003, pp. 2619-2625.
- [11] G. Monti and L. Tarricone, "Negative Group Velocity in a Split Ring Resonator-Coupled Microstrip Line," *Progress In Electromagnetics Research*, Vol. 94, pp. 33-47, 2009.
- [12] L. Markley and G. V. Eleftheriades, "Quad-Band Negative-Refractive-Index Transmission-Line Unit Cell with Reduced Group Delay," *Electronics Letters*, Vol. 46, No. 17, Aug. 2010, pp. 1206-1208.
- [13] C. D. Broomfield and J. K. A. Everard, "Broadband Negative Group Delay Networks for Compensation of Oscillators, Filters and Communication Systems," *Electron. Lett.*, Vol. 36, No. 23, pp. 1931-1933, Nov. 2000.
- [14] M. Kandic, and G. E. Bridges, "Asymptotic limits of negative group delay in active resonator-based distributed circuits," *IEEE Trans. CAS I: Regular Papers*, vol. 58, no. 8, pp. 1727-1735, Aug. 2011.
- [15] C.-T.-M. Wu and T. Itoh, "Maximally flat negative group-delay circuit: A microwave transversal filter approach," *IEEE Trans. Microw. Theory Techn.*, vol. 62, no. 6, pp. 1330-1342, Jun. 2014.
- [16] G. Liu and J. Xu, "Compact transmission-type negative group delay circuit with low attenuation," *Electron. Lett.*, vol. 53, no. 7, pp. 476-478, Mar. 2017.
- [17] T. Shao, Z. Wang, S. Fang, H. Liu, and S. Fu, "A compact transmission line self-matched negative group delay microwave circuit," *IEEE Access*, vol. 5, no. 1, pp. 22836-22843, Oct. 2017.
- [18] T. Shao, S. Fang, Z. Wang and H. Liu, "A Compact Dual-Band Negative Group Delay Microwave Circuit," *Radio Engineering*, vol. 27, no. 4, pp. 1070-1076, Dec. 2018.
- [19] L.-F. Qiu, L.-S. Wu, W.-Y. Yin, and J.-F. Mao, "Absorptive bandstop filter with prescribed negative group delay and bandwidth," *IEEE Microw. Wireless Compon. Lett.*, vol. 27, no. 7, pp. 639-641, Jul. 2017.
- [20] Z. Wang, Y. Cao, T. Shao, S. Fang and Y. Liu, "A Negative Group Delay Microwave Circuit Based on Signal Interference Techniques," *IEEE Microw. Wireless Compon. Lett.*, vol. 28, no. 4, pp. 290-292, Apr. 2018.
- [21] M. W. Mitchell, and R. Y. Chiao, "Negative group delay and "fronts" in a causal system: An experiment with very low frequency bandpass amplifiers," *Phys. Lett. A*, vol. 230, no. 3-4, June 1997, pp. 133-138.
- [22] M. W. Mitchell and R.Y. Chiao, "Causality and Negative Group-delays in a Simple Bandpass Amplifier," *Am. J. Phys.*, vol. 66, 1998, pp. 14-19.
- [23] T. Nakanishi, K. Sugiyama and M. Kitano, "Demonstration of Negative Group-delays in a Simple Electronic Circuit," *Am. J. Phys.*, vol. 70, no. 11, 2002, pp. 1117-1121.
- [24] M. Kitano, T. Nakanishi and K. Sugiyama, "Negative Group-delay and Superluminal Propagation: An Electronic Circuit Approach," *IEEE J. Sel. Top. in Quantum Electron.*, vol. 9, no. 1, Feb. 2003, pp. 43-51.
- [25] J. N. Munday and R. H. Henderson, "Superluminal Time Advance of a Complex Audio Signal," *Appl. Phys. Lett.*, vol. 85, no. 3, July 2004, pp. 503-504.
- [26] B. Ravelo, "Similitude between the NGD function and filter gain behaviours," *Int. J. Circ. Theor. Appl.*, vol. 42, no. 10, Oct. 2014, pp. 1016-1032.
- [27] B. Ravelo, "First-order low-pass negative group delay passive topology," *Electron. Lett.*, vol. 52, no. 2, Jan. 2016, pp. 124-126.
- [28] B. Ravelo, "High-Pass Negative Group Delay RC-Network Impedance," *IEEE Trans. CAS II: Express Briefs*, vol. 64, no. 9, Sept. 2017, pp. 1052-1056.
- [29] B. Ravelo, S. Ngoho, G. Fontgalland, L. Rajaoarisoa, W. Rahajandraibe, R. Vauché, Z. Xu, F. Wan, J. Ge, and S. Lalléchère, "Original Theory of NGD Low Pass-High Pass Composite Function for Designing Inductorless BP-NGD Lumped Circuit," *IEEE Access*, Vol. 8, No. 1, Oct. 2020, pp. 192951-192964.
- [30] B. Ravelo, F. Wan, J. Nebhen, W. Rahajandraibe, and S. Lalléchère, "Resonance Effect Reduction with Bandpass Negative Group Delay Fully Passive Function," *IEEE Transactions on Circuits and Systems II: Express Briefs*, Vol. 68, No. 7, July 2021, pp. 2364-2368.
- [31] B. Ravelo, W. Rahajandraibe, Y. Gan, F. Wan, N. M. Murad and A. Douyère, "Reconstruction Technique of Distorted Sensor Signals with Low-Pass NGD Function," *IEEE Access*, Vol. 8, No. 1, Dec. 2020, pp. 92182-92195.